Current-Induced Dynamics of the Antiferromagnetic Skyrmion and Skyrmionium

Laichuan Shen,[1] Xiaoguang Li,[1] Yuelei Zhao,[2] Jing Xia,[1] Guoping Zhao,[3,*] and Yan Zhou[1,†]

[1] *School of Science and Engineering, The Chinese University of Hong Kong, Shenzhen, Guangdong 518172, China*
[2] *King Abdullah University of Science and Technology (KAUST), Thuwal 23955-6900, Saudi Arabia*
[3] *College of Physics and Electronic Engineering, Sichuan Normal University, Chengdu 610068, China*

(Received 2 September 2019; revised manuscript received 12 November 2019; published 12 December 2019)

Antiferromagnetic (AFM) skyrmionium composed of two topological AFM skyrmions shares the merits of an AFM skyrmion, for example, high mobility and no skyrmion Hall effect. Here, we analytically and numerically study the dynamics of the AFM skyrmion and skyrmionium induced by spin currents. Our calculations demonstrate that the current-induced spin-transfer torques can drive AFM skyrmion and skyrmionium with the same speed, while their steady motion speeds induced by spin-orbit torques are different. Furthermore, it is found that due to the existence of the effective AFM texture mass, the AFM skyrmion and skyrmionium obey the momentum theorem, and the time evolution of the position induced by alternating currents presents a phase. Besides, a spin torque nano-oscillator based on the AFM skyrmionium can produce high frequencies, similar to that based on the AFM skyrmion. Numerical simulations are in good agreement with the analytical solutions. Our results demonstrate the inertial dynamics of the AFM skyrmion and skyrmionium and may provide guidelines for building skyrmion-based spintronic devices.

DOI: 10.1103/PhysRevApplied.12.064033

I. INTRODUCTION

Topologically protected magnetic skyrmions with low depinning current and small size have attracted a great deal of attention [1–11]. In addition, the skyrmionium, which is composed of two coaxial skyrmions with opposite topological charges $Q = +1$ and -1, is also currently a hot topic [12–23], because it has a net topological charge $Q = 0$, resulting in zero skyrmion Hall effect [24,25]. The existence of magnetic skyrmioniums has been experimentally reported [12–14], and they can be controlled by spin currents [15,19], magnetic field gradients [18], magnetic anisotropy gradients [22], and spin waves [20,21].

On the other hand, antiferromagnets are promising materials for advanced spintronic devices due to their ultrafast magnetization dynamics and zero stray fields [26–28]. Similar to ferromagnetic (FM) textures, antiferromagnetic (AFM) textures, such as AFM domain walls and skyrmions, can be controlled by various methods, for instance, spin currents [29–33], magnetic fields [34–37], magnetic anisotropy gradients [38,39], temperature gradients [34,40,41], and spin waves [42–44]. Recently, the stabilization of AFM skyrmions at room temperature has been experimentally presented in synthetic antiferromagnets [45]. Compared to their FM counterparts, AFM skyrmions and skyrmioniums have faster speed and naturally do not show the skyrmion Hall effect due to the cancellation of the Magnus forces [32,33,46–49]. Thus, both of them are ideal information carriers in racetrack-type memory.

For the AFM systems, from two coupled first-order equations with respect to time, one can obtain a second-order equation for the AFM order parameter (Néel vector) [26,50]. Therefore, there is an effective mass of AFM textures and their motion equation should be similar to Newton's kinetic equation. As reported in Ref. [51], since the AFM skyrmions obey the inertial dynamics, the AFM skyrmion-based spin torque nano-oscillators can produce high frequencies (tens of gigahertz). In addition, the alternating-current-induced motion of the AFM bimeron is the well-known Duffing equation, which describes the oscillation of an object with mass [52]. The bimeron can be regarded as the counterpart of the skyrmion in systems with in-plane anisotropy [53,54]. For the AFM skyrmions and skyrmioniums, however, in-depth study of their inertial dynamics is still lacking.

In this work, we analytically and numerically study the dynamics of the AFM skyrmion and skyrmionium induced by spin currents, and we explore their possible applications. We demonstrate that the AFM skyrmion and skyrmionium have the same speeds induced by spin-transfer torques; while using spin-orbit torques to drive them, their steady motion speeds exhibit a difference.

*zhaogp@uestc.edu.cn
†zhouyan@cuhk.edu.cn

Besides, our results show that both the AFM skyrmion and skyrmionium obey inertial dynamics due to the existence of the effective mass. The numerical simulations are in good agreement with our analytical solution.

II. MODEL AND THEORY

We consider a two-sublattice AFM film with perpendicular magnetic anisotropy. From the classical Heisenberg Hamiltonian, the AFM energy E can be written in the following continuous form [55]:

$$E = \int dV \left\{ \frac{\lambda}{2}\boldsymbol{m}^2 + \frac{A}{2}\left[(\nabla \boldsymbol{n})^2 + \partial_x \boldsymbol{n} \cdot \partial_y \boldsymbol{n}\right] + L\boldsymbol{m} \cdot (\partial_x \boldsymbol{n} + \partial_y \boldsymbol{n}) + \frac{K}{2}(1 - n_z^2) + w_D \right\}, \quad (1)$$

where λ, A, L, and K are the homogeneous exchange constant, inhomogeneous exchange constant, parity-breaking constant [30,42,55], and magnetic anisotropy constant, respectively. w_D is the Dzyaloshinskii-Moriya interaction (DMI) energy density, $w_D = (D/2)\boldsymbol{n} \cdot (\nabla \times \boldsymbol{n})$ with the DMI constant D [56–58]. Such a DMI energy is employed to stabilize the Bloch-type skyrmion and skyrmionium. $\boldsymbol{n} = (\boldsymbol{m}_1 - \boldsymbol{m}_2)/2$ and $\boldsymbol{m} = (\boldsymbol{m}_1 + \boldsymbol{m}_2)/2$ are the staggered magnetization (or Néel vector) and the total magnetization, respectively, where $\boldsymbol{m}_i = \boldsymbol{M}_i/M_S$ with M_S being the saturation magnetization. For realistic cases where the antiferromagnetic exchange interaction is significantly strong, $\boldsymbol{m}^2 \ll \boldsymbol{n}^2 \sim 1$ [37].

Taking the current-induced spin torques into account, the evolution of $\boldsymbol{m}$ and $\boldsymbol{n}$ is controlled by the following two coupled equations [29–31,55,59]:

$$\dot{\boldsymbol{n}} = (\gamma \boldsymbol{f}_m - \alpha \dot{\boldsymbol{m}}) \times \boldsymbol{n} + \boldsymbol{T}_{n,\mathrm{SOT}} + \boldsymbol{T}_{n,\mathrm{STT}}, \quad (2a)$$

$$\dot{\boldsymbol{m}} = (\gamma \boldsymbol{f}_n - \alpha \dot{\boldsymbol{n}}) \times \boldsymbol{n} + \boldsymbol{T}_{nl} + \boldsymbol{T}_{m,\mathrm{SOT}} + \boldsymbol{T}_{m,\mathrm{STT}}, \quad (2b)$$

where γ and α are the gyromagnetic ratio and the damping constant, and $\boldsymbol{f}_m = -\delta E/\mu_0 M_S \delta \boldsymbol{m}$ and $\boldsymbol{f}_n = -\delta E/\mu_0 M_S \delta \boldsymbol{n}$ are the effective fields. $\boldsymbol{T}_{nl} = (\gamma \boldsymbol{f}_m - \alpha \dot{\boldsymbol{m}}) \times \boldsymbol{m}$ is the higher-order nonlinear term [29]. $\boldsymbol{T}_{n,\mathrm{SOT}} = \gamma H_j \boldsymbol{m} \times \boldsymbol{p} \times \boldsymbol{n}$ and $\boldsymbol{T}_{m,\mathrm{SOT}} = \gamma H_j \boldsymbol{n} \times \boldsymbol{p} \times \boldsymbol{n}$ are dampinglike spin-orbit torques (SOTs), where the polarization vector $\boldsymbol{p} = \boldsymbol{e_x}$ is employed to drive the skyrmion and skyrmionium. H_j represents the strength of SOTs, which is defined as $H_j = j\hbar P/2\mu_0 e M_S t_z$ with the applied current density j, the reduced Planck constant $\hbar$, the spin polarization rate P, the vacuum permeability constant μ_0, the elementary charge e, and the layer thickness t_z. $\boldsymbol{T}_{n,\mathrm{STT}} = \gamma\eta\partial_x \boldsymbol{n}$ and $\boldsymbol{T}_{m,\mathrm{STT}} = \gamma\beta\partial_x \boldsymbol{n} \times \boldsymbol{n}$ are spin-transfer torques (STTs) with the adiabatic (nonadiabatic) parameter η (β). $\eta = 0.1\beta$ and $\beta = -H_j t_z$ are adopted in this work. Equations (2a) and (2b) do not take into account the thermal fluctuations, so that the results we present are obtained at zero temperature. In order to study the effect of thermal fluctuations, the stochastic thermal field should be introduced to the dynamic equation [33,34,60,61].

We now study the static magnetic structure of the AFM skyrmion and skyrmionium. Substituting $\boldsymbol{f}_m = -(\lambda/\mu_0 M_S)\boldsymbol{m} - (L/\mu_0 M_S)(\partial_x \boldsymbol{n} + \partial_y \boldsymbol{n})$ into Eq. (2a) and supposing $1 + \alpha^2 \sim 1$, the total magnetization $\boldsymbol{m}$ is obtained as

$$\boldsymbol{m} = \frac{\mu_0 M_S}{\gamma\lambda}\dot{\boldsymbol{n}} \times \boldsymbol{n} - \frac{L}{\lambda}(\partial_x \boldsymbol{n} + \partial_y \boldsymbol{n}) - \frac{\alpha\mu_0 M_S}{\lambda}\boldsymbol{f}_n \times \boldsymbol{n}. \quad (3)$$

Equation (3) indicates that the total magnetization depends on the spatial variation of the Néel vector [55]. On the other hand, based on Eqs. (2b) and (3), we get the equation containing only the Néel vector,

$$\frac{\mu_0 M_S}{\gamma\lambda}\ddot{\boldsymbol{n}} \times \boldsymbol{n} - \frac{L}{\lambda}\partial_t \dot{\boldsymbol{n}} = \frac{L}{\lambda}\partial_t \dot{\boldsymbol{n}} \times \boldsymbol{n} \times \boldsymbol{n} + \gamma \boldsymbol{f}_n^* \times \boldsymbol{n} - \alpha \dot{\boldsymbol{n}} \times \boldsymbol{n}, \quad (4)$$

where the dissipation term $(\alpha\mu_0 M_S/\lambda)\dot{\boldsymbol{f}}_n$ has been ignored, because it is weak compared to $\alpha\dot{\boldsymbol{n}}$ [62]. $\boldsymbol{f}_n^* = (A^*/\mu_0 M_S)\Delta\boldsymbol{n} + (K/\mu_0 M_S)n_z \boldsymbol{e_z} - (D/\mu_0 M_S)[\partial_y n_z \boldsymbol{e_x} - \partial_x n_z \boldsymbol{e_y} + (\partial_x n_y - \partial_y n_x)\boldsymbol{e_z}]$ with $A^* = A/2$. $\lambda = 4A/a^2$ and $L = \sqrt{2}A/a$ with the lattice constant a of 0.418 nm [33]. For a static magnetic structure, $\ddot{\boldsymbol{n}} = \boldsymbol{0}$, $\dot{\boldsymbol{n}} = \boldsymbol{0}$, and then Eq. (4) is simplified as $\boldsymbol{f}_n^* \times \boldsymbol{n} = \boldsymbol{0}$, from which a differential equation for $\theta(r)$ is given as

$$\frac{d^2\theta}{dr^2} + \frac{1}{r}\frac{d\theta}{dr} = \left(\frac{1}{r^2} + \frac{K}{A^*}\right)\sin\theta\cos\theta - \frac{D\sin^2\theta}{A^* r}, \quad (5)$$

where $\boldsymbol{n} = -\sin\theta\sin\varphi\boldsymbol{e_x} + \sin\theta\cos\varphi\boldsymbol{e_y} + \cos\theta\boldsymbol{e_z}$ has been taken into account. Equation (5) can be used to identify the skyrmions and skyrmioniums in AFM systems. Similar to the case of the FM skyrmion [56], the profile of the AFM skyrmion can be obtained by solving Eq. (5). In addition, taking $\theta(r = 0) = 0$ and scanning $d\theta/dr(r = 0)$, Eq. (5) gives different angles θ_b on the nanodisk edge. The corresponding AFM energies are calculated using Eq. (1) [see Fig. 1(a)]. A similar method to calculate the energy curve has been reported [63], and the AFM energy curves for different DMI constants are plotted in Ref. [60]. As shown in Fig. 1(a), there are three minimal energy values, corresponding to the quasiuniform AFM state (QAFM), AFM skyrmion, and AFM skyrmionium. Their Néel vector profiles are plotted in Fig. 1(b), where the lines are given by Eq. (5), while the symbols are obtained from numerical simulations with the DMI-induced boundary condition $d\boldsymbol{n}/dr = (D/2A^*)\boldsymbol{e_r} \times \boldsymbol{n}$ [56]. By considering the symmetry of the AFM skyrmion and skyrmionium and combining Eq. (3), their magnetic structures can be obtained (see Ref. [60]).

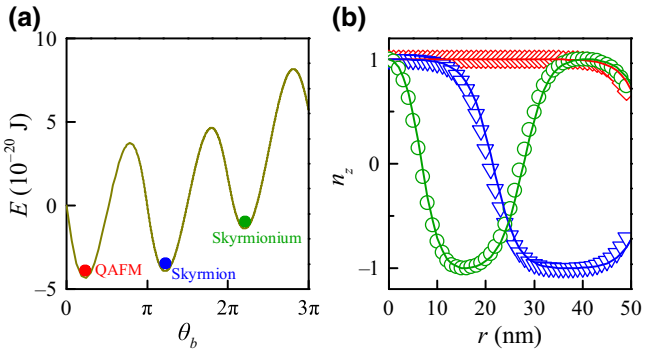

FIG. 1. (a) The AFM energy E as a function of the angle θ_b on the nanodisk edge, where there are three minimal energy values, which correspond to the quasiuniform AFM state (QAFM), AFM skyrmion, and AFM skyrmionium. (b) The profile $n_z = \cos\theta$ for the quasiuniform AFM state, AFM skyrmion, and AFM skyrmionium, where the symbols are the simulation results, and the lines are obtained by solving Eq. (5). In our simulations, the following parameters are adopted [33]: $A = 6.59$ pJ/m, $K = 0.116$ MJ/m^3, $D = 0.8$ mJ/m^2, $M_S = 376$ kA/m, $\lambda = 150.9$ MJ/m^3, $L = 22.3$ mJ/m^2, $\gamma = 2.211 \times 10^5$ m/(A s), and $\alpha = 0.2$. The mesh size of $1 \times 1 \times 1$ nm^3 is used to discretize the AFM nanodisk with a radius of 50 nm and thickness of 1 nm.

III. THE MOTION OF THE AFM SKYRMION AND SKYRMIONIUM DRIVEN BY CURRENTS

In this part, we derive the steady motion equations for the rigid AFM skyrmion and skyrmionium using Thiele's (or the collective coordinate) approach [62,64–66]. By adding $\boldsymbol{T}_{m,\mathrm{SOT}}$ and $\boldsymbol{T}_{m,\mathrm{STT}}$ to Eq. (4), and taking the cross product with $\boldsymbol{n}$, we get

$$\frac{\mu_0 M_S}{\gamma\lambda}\ddot{\boldsymbol{n}} \times \boldsymbol{n} \times \boldsymbol{n} = \gamma \boldsymbol{f}_n^* \times \boldsymbol{n} \times \boldsymbol{n} + \alpha\dot{\boldsymbol{n}} - \gamma H_j \boldsymbol{n} \times \boldsymbol{p} - \gamma\beta\partial_x \boldsymbol{n}. \tag{6}$$

Then, taking the scalar product with $\partial_i \boldsymbol{n}$ and integrating over the space, the Thiele equation is derived as

$$\boldsymbol{a} \cdot \boldsymbol{M}_{\mathrm{eff}} = \boldsymbol{F}_\alpha + \boldsymbol{F}_{\mathrm{SOT}} + \boldsymbol{F}_{\mathrm{STT}}, \tag{7}$$

where $\boldsymbol{a}$ is the acceleration and $\boldsymbol{M}_{\mathrm{eff}}$ is the effective AFM texture mass, which is defined as $\mu_0^2 M_S^2 t_z \boldsymbol{d}/\gamma^2\lambda$ with the dissipative tensor $\boldsymbol{d}$. The components d_{ij} of the dissipative tensor are $d_{xx} = d_{yy} = d = \int dx\,dy\,(\partial_x \boldsymbol{n} \cdot \partial_x \boldsymbol{n})$ and $d_{xy} = d_{yx} = 0$. The effective AFM texture mass is intrinsic, since it follows from the existence of two sublattices [26]. Note that other factors contributing to the skyrmion inertia, such as the boundary effects [67] and the magnon modes in the continuum [68], have not been taken into account. $\boldsymbol{F}_\alpha = -\alpha\mu_0 M_S t_z \boldsymbol{v} \cdot \boldsymbol{d}/\gamma$ represents the dissipative force with the velocity $\boldsymbol{v}$. $\boldsymbol{F}_{\mathrm{SOT}} = F_{\mathrm{SOT},x}\boldsymbol{e_x} + F_{\mathrm{SOT},y}\boldsymbol{e_y}$ with $F_{\mathrm{SOT},i} = -\mu_0 H_j M_S t_z \int dx\,dy[(\boldsymbol{n} \times \boldsymbol{p}) \cdot \partial_i \boldsymbol{n}]$ and $\boldsymbol{F}_{\mathrm{STT}} = -\mu_0 M_S \beta t_z d \boldsymbol{e_x}$ are the forces induced by SOTs and STTs, respectively. The steady motion of the AFM skyrmion and skyrmionium leads to $\boldsymbol{a} = \boldsymbol{0}$, and Eq. (7) gives the steady motion speed,

$$v = -\gamma \frac{H_j u}{\alpha d} - \gamma \frac{\beta}{\alpha}, \tag{8}$$

where $u = \int dx\,dy[(\boldsymbol{n} \times \boldsymbol{p}) \cdot \partial_i \boldsymbol{n}]$, and the first and second terms on the right side of Eq. (8) are the SOT- and STT-induced speeds, respectively. Since the dissipative and STT-induced forces are proportional to the component d of the dissipative tensor, the d involved in the magnetic structure is offset in the process of deriving the steady motion speed. Therefore, the AFM skyrmion and skyrmionium should have the same speeds driven by STTs. However, the physical quantities involved in the magnetic structure cannot be offset for the case of SOTs, so that the SOT-induced speeds are different for the AFM skyrmion and skyrmionium. In addition, the motion speed is inversely proportional to the damping constant for SOTs and STTs.

In order to visually show the relation between the SOT-induced speed and the physical quantities, we derive the analytical formula of u. Taking $\boldsymbol{n} = -\sin\theta\sin\varphi\boldsymbol{e_x} + \sin\theta\cos\varphi\boldsymbol{e_y} + \cos\theta\boldsymbol{e_z}$ for an AFM skyrmion and considering $\boldsymbol{p} = \boldsymbol{e_x}$, we rewrite u in polar coordinates (r, φ), $u = \int \left[\cos^2\varphi(d\theta/dr) + \sin\theta\cos\theta\sin^2\varphi/r\right] r\,dr\,d\varphi$. The integral for the second term is small, so that it can be ignored. Using the assumption, i.e., $d\theta/dr \neq 0$ only for $r \approx R_s$, we obtain the value of $u \approx -\pi^2 R_s$ with skyrmion radius R_s. Therefore, Eq. (8) becomes

$$v = \gamma \frac{\pi^2 R_s H_j}{\alpha d} - \gamma \frac{\beta}{\alpha}. \tag{9}$$

Equation (9) shows that for a larger AFM skyrmion, the SOT-induced motion speed increases.

To verify the above analytical results, we simulate the motion of the AFM skyrmion and skyrmionium based on Eqs. (2a) and (2b), where the relaxed AFM skyrmion (or skyrmionium) is the initial state. Figures 2(a)–2(d) show the evolution of velocity for the AFM skyrmion and skyrmionium induced by SOTs and STTs, where we set $j = 5$ MA/cm^2 and $\alpha = 0.01$. The velocity components are $(v_x, v_y) = (\dot{r}_x, \dot{r}_y)$, where the guiding center (r_x, r_y) of the skyrmion is defined as [19]

$$r_i = \frac{1}{4\pi Q}\int i\boldsymbol{n} \cdot (\partial_x \boldsymbol{n} \times \partial_y \boldsymbol{n}) dx\,dy, \quad i = x, y. \tag{10}$$

Q ($= \pm 1$ for an isolated AFM skyrmion) is the AFM topological charge, which is written as $Q = \frac{1}{4\pi}\int dx\,dy[\boldsymbol{n} \cdot (\partial_x \boldsymbol{n} \times \partial_y \boldsymbol{n})]$ [33,69,70]. On the other hand, for the AFM

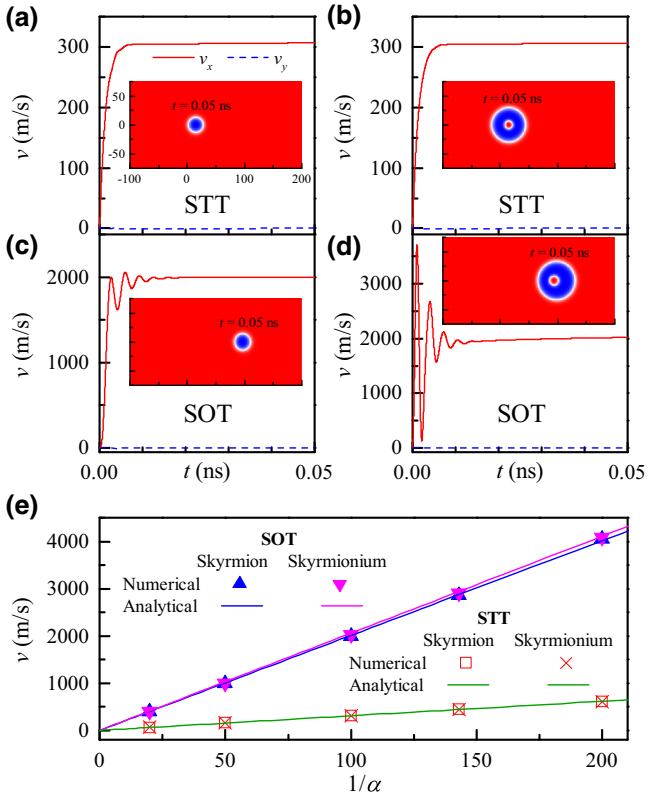

FIG. 2. (a)–(d) The evolution of velocity (v_x, v_y) for the AFM skyrmion and skyrmionium induced by SOTs and STTs, where $\alpha = 0.01$, $P = 0.4$, $D = 0.7$ mJ/m^2, and $j = 5$ MA/cm^2 are adopted in our simulations. The insets show the top views of the AFM skyrmion and skyrmionium at $t = 0.05$ ns. (e) The velocities at $t = 0.05$ ns as functions of $1/\alpha$, where the symbols are obtained from the numerical simulations, while the lines are the analytical results given by Eq. (8) with numerical values of $u \sim -1.33 \times 10^{-7}$ m $(-3.91 \times 10^{-7}$ m) and $d \sim 20.4$ (58.6) for the skyrmion (skyrmionium) [60].

skyrmionium, we use the following formula [19]:

$$r_i = \frac{\int i(1-n_z)dx\,dy}{\int (1-n_z)dx\,dy}, \quad i = x, y. \tag{11}$$

Figure 2 shows that the AFM skyrmion and skyrmionium have the same steady motion speeds of 306 m/s for STTs, and they do not show obvious deformations. For SOTs, however, the evolution of their speeds is different, and the difference increases with currents [60]. In addition, a shift for the skyrmionium core can be observed, as shown by the inset of Fig. 2(d). Since the size of the skyrmionium shell is larger than that of the skyrmionium core, Eq. (9) indicates that the shell moves faster than the core, resulting in the shift of the core relative to the shell. Compared to AFM skyrmioniums, FM skyrmioniums exhibit different motion behavior. As reported in Refs. [15,16], since the FM skyrmionium core and shell have opposite topological charges $+1$ and -1, the Magnus forces acting on them have the opposite directions. Therefore, the drift direction is downward for the core and upward for the shell, resulting in the stretching and deformation of the FM skyrmionium. Besides, the speed of FM skyrmioniums (approximately 150 m/s) [15,16] is smaller than that of AFM skyrmioniums (a few kilometers per second). On the other hand, the AFM skyrmion and skyrmionium do not show any transverse drift. As shown in Fig. 2(e), the motion speeds of the AFM skyrmion and skyrmionium are inversely proportional to the damping constants, and the numerical simulations are in good agreement with Eq. (8).

When the alternating current $j = j_0 \cos(2\pi ft)$ with amplitude $j_0 = 5$ MA/cm^2 and frequency $f = \sim 5$–20 GHz is adopted as the driving source, the AFM skyrmion and skyrmionium show the stable oscillation with amplitude r_0 and phase difference ψ between r_x and $\sin(2\pi ft)$ [60]. Figure 3 shows that as the frequency f increases, the amplitude r_0 goes down, and the phase ψ becomes larger. Next, based on the Thiele equation, we analyze the simulation results. Equation (7) can be rewritten as a scalar equation $M_{\rm eff}\ddot{r}_x + \alpha^* \dot{r}_x = F_{\rm STT,0} \cos(2\pi ft)$ with $\alpha^* = \alpha\mu_0 M_S t_z d/\gamma$ and $F_{\rm STT,0} = \mu_0 M_S \beta t_z d$. Such a scalar equation describes the forced oscillation of an object, and its solution can be written as $r_x = r_0 \sin(2\pi ft - \psi)$, where the amplitude r_0 is

$$r_0 = \frac{F_{\rm STT,0}}{2\pi f \sqrt{(2\pi f M_{\rm eff})^2 + \alpha^{*2}}}, \tag{12}$$

and the phase ψ is equal to

$$\psi = \arctan(2\pi f M_{\rm eff}/\alpha^*) = \arctan(2\pi f\, \mu_0 M_S/\alpha\gamma\lambda). \tag{13}$$

Equation (13) shows that the phase is due to the existence of the effective mass, and for the same parameters, the AFM skyrmion and skyrmionium have the same phase. In

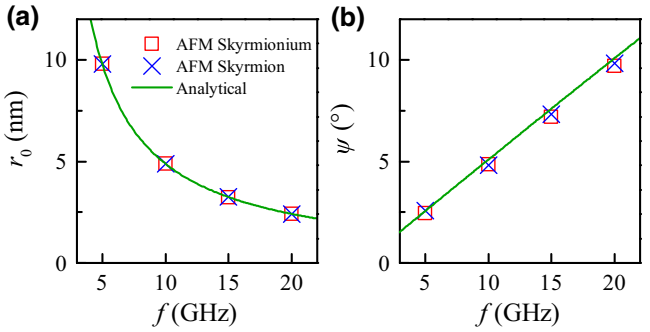

FIG. 3. (a) The amplitude r_0 and (b) phase ψ as functions of the frequency f of alternating currents $[j = j_0 \cos(2\pi ft)]$, where $j_0 = 5$ MA/cm^2, $\alpha = 0.01$, and current-induced STTs are considered. Symbols are the results of our numerical simulations, while lines are obtained from Eqs. (12) and (13).

addition, Eq. (12) indicates that the AFM skyrmion and skyrmionium exhibit the same amplitude driven by STTs, as shown in Fig. 3.

IV. MOMENTUM THEOREM FOR THE AFM SKYRMION AND SKYRMIONIUM

The Thiele equation, i.e., Eq. (7), shows that the AFM skyrmion and skyrmionium have an effective mass, so that they should obey the momentum theorem. The current is switched off when the AFM skyrmion and skyrmionium are accelerated to 500 m/s via current-induced STT. As shown in Figs. 4(a) and 4(b), the motion speeds will decrease due to the existence of the damping, and interestingly, the AFM skyrmion and skyrmionium have the same motion behaviors. Next, we employ the momentum theorem to analyze the above results. Using $M_{\text{eff}}\,dv = F_\alpha\,dt$ with $F_\alpha = -\alpha^* v$, we get $\ln(v_0/v_1) = (\alpha^*/M_{\text{eff}})(t_1 - t_0)$. Taking $v_0 = 500$ m/s at $t_0 = 0$ and $v_1 = 183.94$ m/s at t_1, t_1 is derived as

$$t_1 = M_{\text{eff}}/\alpha^* = \mu_0 M_S/\alpha\gamma\lambda. \tag{14}$$

Equation (14) shows that for the same parameters, the AFM skyrmion and skyrmionium have the same time t_1, which is consistent with the simulation result [see Figs. 4(a) and 4(b)]. In addition, as shown in Fig. 4(c), t_1 is inversely proportional to the damping constant.

Considering that there are two AFM skyrmions (labeled A and B; see Fig. 5) or skyrmioniums in the racetrack, they still obey the momentum theorem, i.e., $M_{\text{eff}}\,dv_{\text{A}} + M_{\text{eff}}\,dv_{\text{B}} = -\alpha^* v_{\text{A}}\,dt - \alpha^* v_{\text{B}}\,dt$. Based on the preceding equation, the evolution of the total speed $v_t = v_{\text{A}} + v_{\text{B}}$ is

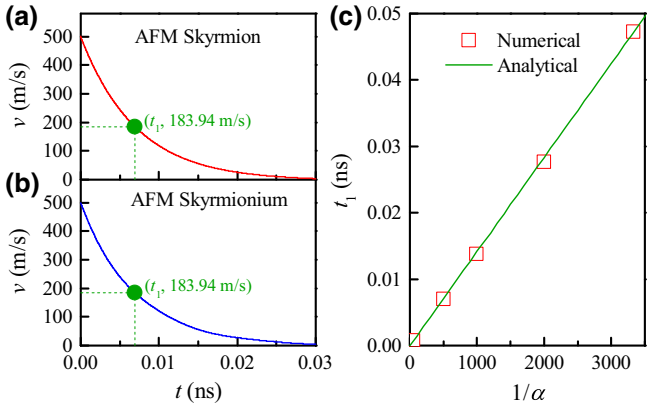

FIG. 4. (a),(b) The evolution of motion speeds for the AFM skyrmion and skyrmionium, where they have an initial speed of 500 m/s, the driving source is not applied, and the damping α is set to be 0.002 in our simulations. For the AFM skyrmion and skyrmionium, when the speed goes down from 500 m/s to 183.94 m/s, it takes the same time of $t_1 \sim 0.00695$ ns. (c) The time t_1 as a function of $1/\alpha$, where the symbols are the simulation results, while the line is given by Eq. (14).

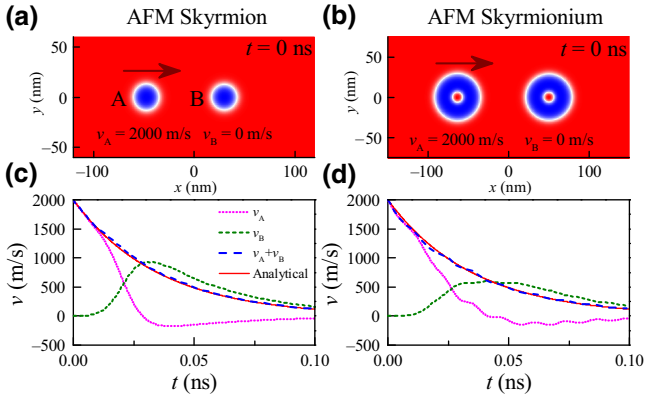

FIG. 5. (a),(b) The top views of two AFM skyrmions and skyrmioniums at $t = 0$ ns, where the AFM skyrmion and skyrmionium on the left have an initial speed of 2000 m/s, while they are stationary on the right. (c),(d) The evolution of motion speeds for two AFM skyrmions and skyrmioniums, where the driving source is not applied and the damping α is set to be 0.0004 in our simulations. Dashed lines denote the results of our numerical simulations, while solid lines are given by Eq. (15).

obtained as

$$v_t = v_{\text{A}} + v_{\text{B}} = v_{t,0}\exp(-\alpha^* t/M_{\text{eff}}). \tag{15}$$

When the AFM skyrmion labeled A is accelerated to 2000 m/s by STT, we turn off the current and put the AFM skyrmion labeled B in the racetrack, as shown in Fig. 5(a). Then, the collision of the two AFM skyrmions will occur, resulting in that the AFM skyrmion B achieves a certain speed. We can see from Fig. 5(c) that the total speed $v_{\text{A}} + v_{\text{B}}$ of the numerical simulation (blue dashed line) agrees well with the result of Eq. (15) (red solid line). For AFM skyrmioniums, Eq. (15) is also applicable [see Fig. 5(d)].

V. APPLICATIONS OF THE AFM SKYRMION AND SKYRMIONIUM

A. Racetrack-type memory based on the AFM skyrmion and skyrmionium

As shown in Fig. 2, the AFM skyrmion and skyrmionium have ultrafast speeds without showing any transverse drift, so that they are ideal information carriers in racetrack-type memory. The AFM skyrmion-based racetrack is suggested, as shown in Fig. 6(a), where the data information (i.e., digital "1" or "0") is encoded by the presence or absence of an AFM skyrmion. Similar to the case of FM skyrmions [71–73], the distance between two AFM skyrmions may be affected by many factors, such as the thermal fluctuations [33], so that the number of the data bit 0 cannot be accurately encoded. Therefore, it is necessary to explore alternative designs for the data representation. Figure 6(b) shows a possible design, where the data bit 0 is

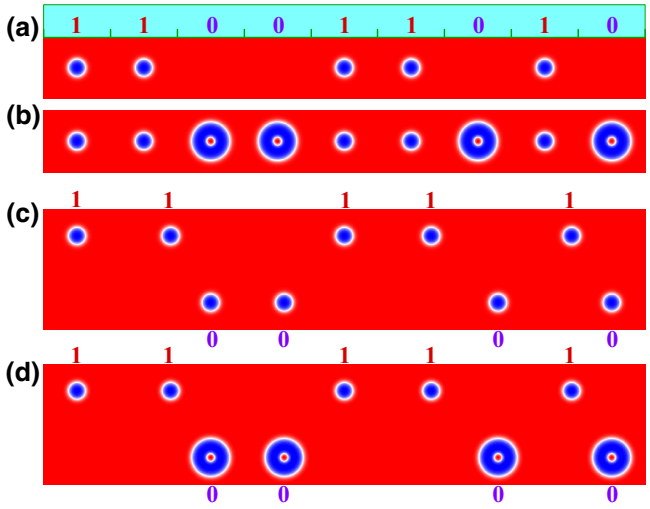

FIG. 6. (a) The representation of data information (i.e., "1" or "0") in the single-lane racetrack, where the presence and absence of an AFM skyrmion are used to encode the data bits 1 and 0, respectively. (b) The alternative design for the data representation, where the data bits 1 and 0 are encoded by the presence of the AFM skyrmion and skyrmionium, respectively. (c),(d) The two-lane racetrack based on the AFM skyrmions (or skyrmioniums), where the top lane is responsible for encoding the data bit 1 and the bottom lane is employed in order to encode the data bit 0.

encoded by the presence of an AFM skyrmionium, instead of the distance between two AFM skyrmions.

On the other hand, in order to accurately encode the data bit 0 in the FM racetrack, an electric-field-controlled Y-junction [72] and two-lane FM racetrack [71,73] have been proposed. However, such schemes require sophisticated reprocessing and are not favorable from the point of view of device applications. For instance, in the two-lane FM racetrack, a high energy barrier, which can be induced by applying high magnetic anisotropy [73] or using an additional nanostrip [71], needs to be introduced between the lanes to eliminate the data confusion caused by the skyrmion Hall effect. For the AFM skyrmion and skyrmionium, due to the cancellation of the Magnus force, their motion trajectory is a perfectly straight line along the racetrack, so that they are favorable in racetrack-type memory and two or multiple lanes in an AFM racetrack can be built, as shown in Figs. 6(c) and 6(d). In two-lane AFM racetracks, the presence of an AFM skyrmion (or skyrmionium) in the top and bottom lanes is used to encode the data bits 1 and 0, respectively. Such a design for the data representation is robust, since we always detect an AFM skyrmion (or skyrmionium) for the data bits 1 and 0, similar to the case of the FM skyrmion [72]. Obviously, the two-lane racetrack will increase the size of devices in practical applications, compared to the single-lane AFM racetrack.

B. Spin torque nano-oscillators based on the AFM skyrmionium

Recently, spin torque nano-oscillators (STNOs) based on magnetic skyrmions have received great attention due to their important role in modern microwave generators [51,74–77]. For FM skyrmion-based STNOs, the oscillation frequencies are low (about 1 GHz), since the fast-moving FM skyrmion results in the presence of a large Magnus force and then the skyrmion will be destroyed at the nanodisk edge. In order to overcome this obstacle, the AFM skyrmion-based STNOs are proposed, where the AFM skyrmion obeys the inertial dynamics and the oscillation frequency of the AFM skyrmion (tens of gigahertz) is higher than that of the FM skyrmion, as reported in Ref. [51]. In addition, the skyrmion motion in the AFM nanodisk is independent of the sign of the applied current. For STNOs based on the AFM skyrmionium, the results should be similar to those of STNOs based on the AFM skyrmion.

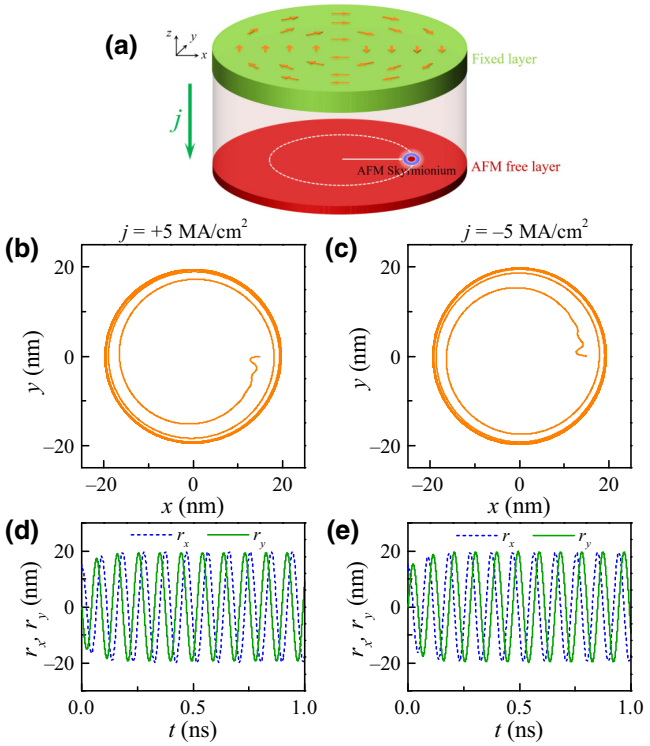

FIG. 7. (a) The sketch of spin torque nano-oscillators based on the AFM skyrmionium. The fixed layer is used to generate the spin-polarized current with a vortexlike polarization. Such a spin-polarized current applies spin torques (the dampinglike SOTs are considered) to the AFM layer, and then the AFM skyrmionium moves in a circular motion. (b),(c) The trajectories of the AFM skyrmionium for $j = 5$ and -5 MA/cm^2. (d),(e) The time evolution of the position (r_x, r_y). In our simulations, the diameter of the AFM nanodisk is 160 nm and the damping α is set to be 0.01.

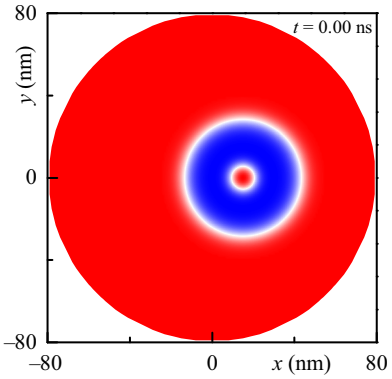

VIDEO 1. An AFM skyrmionium moves in a circular motion, where the adopted parameters are the same as those of Fig. 7(b).

Figure 7 shows that when the spin-polarized current with a vortexlike polarization is applied, the AFM skyrmionium will move in a circular motion. Similar to the AFM skyrmion, the motion of the AFM skyrmionium does not depend on the sign of the current. On the other hand, for the parameters used here, the oscillation frequency of the AFM skyrmionium is approximately 10.6 GHz. It should be noted that compared to the AFM skyrmion in the STNOs [51], the AFM skyrmionium exhibits an obvious deformation (see Video 1).

VI. CONCLUSIONS

In summary, we study the motion of the AFM skyrmion and skyrmionium induced by spin currents, and explore their possible applications. We demonstrate that current-induced STTs can drive the AFM skyrmion and skyrmionium with the same motion speeds, because the physical quantities involved in the magnetic structure are offset for the case of STTs. For SOTs, however, they cannot be offset, and the SOT-induced speeds are different for the AFM skyrmion and skyrmionium. In addition, we discuss the forced oscillation driven by alternating currents, showing that there is a phase due to the existence of the effective mass. Since the phase depends on the physical quantities of antiferromagnets, such as the damping and exchange constants, they may be measured by the phase. Furthermore, we prove that AFM skyrmions and skyrmioniums obey the momentum theorem. Since both AFM skyrmions and skyrmioniums have ultrafast speeds (up to a few kilometers per second) without showing any transverse drift, they are ideal information carriers in racetrack-type memory and one can easily build two-lane AFM racetracks in order to accurately encode the data bits. Moreover, based on the inertial characteristics, the AFM skyrmionium-based spin torque nano-oscillators are proposed and such nano-oscillators can produce high frequencies of approximately 10.6 GHz. Our results are useful for the understanding of the inertial dynamics and the applications of the AFM skyrmion and skyrmionium.

ACKNOWLEDGMENTS

G.Z. acknowledges the support by the National Natural Science Foundation of China (Grants No. 51771127, No. 51571126, and No. 51772004) of China and the Scientific Research Fund of the Sichuan Provincial Education Department (Grants No. 18TD0010 and No. 16CZ0006). Y.Z. acknowledges the support by the President's Fund of CUHKSZ, Longgang Key Laboratory of Applied Spintronics, National Natural Science Foundation of China (Grants No. 11974298 and No. 61961136006), Shenzhen Fundamental Research Fund (Grant No. JCYJ20170410171958839), and Shenzhen Peacock Group Plan (Grant No. KQTD20180413181702403).

Laichuan Shen, Xiaoguang Li, and Yuelei Zhao contributed equally to this work.

[1] U. K. Rößler, A. N. Bogdanov, and C. Pfleiderer, Spontaneous skyrmion ground states in magnetic metals, Nature **442**, 797 (2006).

[2] N. Nagaosa and Y. Tokura, Topological properties and dynamics of magnetic skyrmions, Nat. Nanotechnol. **8**, 899 (2013).

[3] A. Fert, N. Reyren, and V. Cros, Magnetic skyrmions: Advances in physics and potential applications, Nat. Rev. Mat. **2**, 17031 (2017).

[4] G. Finocchio, F. Büttner, R. Tomasello, M. Carpentieri, and M. Kläui, Magnetic skyrmions: From fundamental to applications, J. Phys. D: Appl. Phys. **49**, 423001 (2016).

[5] K. Everschor-Sitte, J. Masell, R. M. Reeve, and M. Kläui, Perspective: Magnetic skyrmions—overview of recent progress in an active research field, J. Appl. Phys. **124**, 240901 (2018).

[6] X. Z. Yu, N. Kanazawa, W. Z. Zhang, T. Nagai, T. Hara, K. Kimoto, Y. Matsui, Y. Onose, and Y. Tokura, Skyrmion flow near room temperature in an ultralow current density, Nat. Commun. **3**, 988 (2012).

[7] W. Kang, Y. Huang, X. Zhang, Y. Zhou, and W. Zhao, Skyrmion-electronics: An overview and outlook, Proc. IEEE **104**, 2040 (2016).

[8] Y. Zhou, Magnetic skyrmions: Intriguing physics and new spintronic device concepts, Natl. Sci. Rev. **6**, 210 (2019).

[9] X. Zhang, M. Ezawa, and Y. Zhou, Magnetic skyrmion logic gates: Conversion, duplication and merging of skyrmions, Sci. Rep. **5**, 9400 (2015).

[10] X. Zhang, G. P. Zhao, H. Fangohr, J. P. Liu, W. X. Xia, J. Xia, and F. J. Morvan, Skyrmion-skyrmion and skyrmion-edge repulsions in skyrmion-based racetrack memory, Sci. Rep. **5**, 7643 (2015).

[11] X. Zhang, Y. Zhou, K. M. Song, T.-E. Park, J. Xia, M. Ezawa, X. Liu, W. Zhao, G. Zhao, and S. Woo, Skyrmion-electronics: Writing, deleting, reading and processing magnetic skyrmions toward spintronic applications, J. Phys.: Condens. Matter (2019).

[12] M. Finazzi, M. Savoini, A. R. Khorsand, A. Tsukamoto, A. Itoh, L. Duò, A. Kirilyuk, Th. Rasing, and M. Ezawa, Laser-Induced Magnetic Nanostructures With Tunable Topological Properties, Phys. Rev. Lett. **110**, 177205 (2013).

[13] F. Zheng, H. Li, S. Wang, D. Song, C. Jin, W. Wei, A. Kovács, J. Zang, M. Tian, Y. Zhang, H. Du, and R. E. Dunin-Borkowski, Direct Imaging of a Zero-Field Target Skyrmion and its Polarity Switch in a Chiral Magnetic Nanodisk, Phys. Rev. Lett. **119**, 197205 (2017).

[14] S. Zhang, F. Kronast, G. van der Laan, and T. Hesjedal, Real-space observation of skyrmionium in a ferromagnet-magnetic topological insulator heterostructure, Nano Lett. **18**, 1057 (2018).

[15] X. Zhang, J. Xia, Y. Zhou, D. Wang, X. Liu, W. Zhao, and M. Ezawa, Control and manipulation of a magnetic skyrmionium in nanostructures, Phys. Rev. B **94**, 094420 (2016).

[16] A. G. Kolesnikov, M. E. Stebliy, A. S. Samardak, and A. V. Ognev, Skyrmionium-high velocity without the skyrmion Hall effect, Sci. Rep. **8**, 16966 (2018).

[17] A. O. Leonov, U. K. Rößler, and M. Mostovoy, Target-skyrmions and skyrmion clusters in nanowires of chiral magnets, EPJ Web Conf. **75**, 05002 (2014).

[18] S. Komineas and N. Papanicolaou, Skyrmion dynamics in chiral ferromagnets, Phys. Rev. B **92**, 064412 (2015).

[19] S. Komineas and N. Papanicolaou, Skyrmion dynamics in chiral ferromagnets under spin-transfer torque, Phys. Rev. B **92**, 174405 (2015).

[20] M. Shen, Y. Zhang, J. Ou-Yang, X. Yang, and L. You, Motion of a skyrmionium driven by spin wave, Appl. Phys. Lett. **112**, 062403 (2018).

[21] S. Li, J. Xia, X. Zhang, M. Ezawa, W. Kang, X. Liu, Y. Zhou, and W. Zhao, Dynamics of a magnetic skyrmionium driven by spin waves, Appl. Phys. Lett. **112**, 142404 (2018).

[22] C. Song, C. Jin, J. Wang, Y. Ma, H. Xia, J. Wang, J. Wang, and Q. Liu, Dynamics of a magnetic skyrmionium in an anisotropy gradient, Appl. Phys. Express **12**, 083003 (2019).

[23] B. Göbel, A. F. Schäffer, J. Berakdar, I. Mertig, and S. S. P. Parkin, Electrical writing, deleting, reading, and moving of magnetic skyrmioniums in a racetrack device, Sci. Rep. **9**, 12119 (2019).

[24] W. Jiang, X. Zhang, G. Yu, W. Zhang, X. Wang, M. Benjamin Jungfleisch, John E. Pearson, X. Cheng, O. Heinonen, K. L. Wang, Y. Zhou, A. Hoffmann, and Suzanne G. E. te Velthuis, Direct observation of the skyrmion Hall effect, Nat. Phys. **13**, 162 (2017).

[25] K. Litzius, I. Lemesh, B. Krüger, P. Bassirian, L. Caretta, K. Richter, F. Büttner, K. Sato, O. A. Tretiakov, J. Förster, R. M. Reeve, M. Weigand, I. Bykova, H. Stoll, G. Schütz, G. S. D. Beach, and M. Kläui, Skyrmion Hall effect revealed by direct time-resolved X-ray microscopy, Nat. Phys. **13**, 170 (2017).

[26] V. Baltz, A. Manchon, M. Tsoi, T. Moriyama, T. Ono, and Y. Tserkovnyak, Antiferromagnetic spintronics, Rev. Mod. Phys. **90**, 015005 (2018).

[27] T. Jungwirth, X. Marti, P. Wadley, and J. Wunderlich, Antiferromagnetic spintronics, Nat. Nanotechnol. **11**, 231 (2016).

[28] L. Šmejkal, Y. Mokrousov, B. Yan, and A. H. MacDonald, Topological antiferromagnetic spintronics, Nat. Phys. **14**, 242 (2018).

[29] K. M. D. Hals, Y. Tserkovnyak, and A. Brataas, Phenomenology of Current-Induced Dynamics in Antiferromagnets, Phys. Rev. Lett. **106**, 107206 (2011).

[30] T. Shiino, S. H. Oh, P. M. Haney, S. W. Lee, G. Go, B. G. Park, and K. J. Lee, Antiferromagnetic Domain Wall Motion Driven by Spin-Orbit Torques, Phys. Rev. Lett. **117**, 087203 (2016).

[31] H. Velkov, O. Gomonay, M. Beens, G. Schwiete, A. Brataas, J. Sinova, and R. A. Duine, Phenomenology of current-induced skyrmion motion in antiferromagnets, New J. Phys. **18**, 075016 (2016).

[32] X. Zhang, Y. Zhou, and M. Ezawa, Antiferromagnetic skyrmion: Stability, creation and manipulation, Sci. Rep. **6**, 24795 (2016).

[33] J. Barker and O. A. Tretiakov, Static and Dynamical Properties of Antiferromagnetic Skyrmions in the Presence of Applied Current and Temperature, Phys. Rev. Lett. **116**, 147203 (2016).

[34] R. Khoshlahni, A. Qaiumzadeh, A. Bergman, and A. Brataas, Ultrafast generation and dynamics of isolated skyrmions in antiferromagnetic insulators, Phys. Rev. B **99**, 054423 (2019).

[35] H. Y. Yuan, W. Wang, M. H. Yung, and X. R. Wang, Classification of magnetic forces acting on an antiferromagnetic domain wall, Phys. Rev. B **97**, 214434 (2018).

[36] O. Gomonay, M. Kläui, and J. Sinova, Manipulating antiferromagnets with magnetic fields: Ratchet motion of multiple domain walls induced by asymmetric field pulses, Appl. Phys. Lett. **109**, 142404 (2016).

[37] S. Dasgupta, S. K. Kim, and O. Tchernyshyov, Gauge fields and related forces in antiferromagnetic soliton physics, Phys. Rev. B **95**, 220407(R) (2017).

[38] L. Shen, J. Xia, G. Zhao, X. Zhang, M. Ezawa, O. A. Tretiakov, X. Liu, and Y. Zhou, Dynamics of the antiferromagnetic skyrmion induced by a magnetic anisotropy gradient, Phys. Rev. B **98**, 134448 (2018).

[39] K. Yamada, K. Kubota, and Y. Nakatani, Magnetic domain wall motion in anti-ferromagnetic nanowires induced by sloped electric field, Appl. Phys. Express **11**, 113001 (2018).

[40] Z. Y. Chen, Z. R. Yan, M. H. Qin, and J.-M. Liu, Landau-Lifshitz-Bloch equation for domain wall motion in antiferromagnets, Phys. Rev. B **99**, 214436 (2019).

[41] S. Selzer, U. Atxitia, U. Ritzmann, D. Hinzke, and U. Nowak, Inertia-Free Thermally Driven Domain-Wall Motion in Antiferromagnets, Phys. Rev. Lett. **117**, 107201 (2016).

[42] A. Qaiumzadeh, L. A. Kristiansen, and A. Brataas, Controlling chiral domain walls in antiferromagnets using spin-wave helicity, Phys. Rev. B **97**, 020402(R) (2018).

[43] E. G. Tveten, A. Qaiumzadeh, and A. Brataas, Antiferromagnetic Domain Wall Motion Induced by Spin Waves, Phys. Rev. Lett. **112**, 147204 (2014).

[44] M. W. Daniels, W. Yu, R. Cheng, J. Xiao, and D. Xiao, Topological spin Hall effects and tunable skyrmion Hall effects in uniaxial antiferromagnetic insulators, Phys. Rev. B **99**, 224433 (2019).

[45] W. Legrand, D. Maccariello, F. Ajejas, S. Collin, A. Vecchiola, K. Bouzehouane, N. Reyren, V. Cros, and A. Fert, Room-temperature stabilization of antiferromagnetic skyrmions in synthetic antiferromagnets, Nat. Mater. (2019).

[46] X. Zhang, Y. Zhou, and M. Ezawa, Magnetic bilayer-skyrmions without skyrmion Hall effect, Nat. Commun. **7**, 10293 (2016).

[47] H. Yang, C. Wang, T. Yu, Y. Cao, and P. Yan, Antiferromagnetism Emerging in a Ferromagnet with Gain, Phys. Rev. Lett. **121**, 197201 (2018).

[48] M. M. M. Bhukta, A. Mishra, G. Pradhan, S. Mallick, B. B. Singh, and S. Bedanta, A novel chiral spin texture: Antiferromagnetic skyrmionium, arXiv:1810.08262.

[49] S. A. Obadero, Y. Yamane, C. A. Akosa, and G. Tatara, Current-driven nucleation and propagation of antiferromagnetic skyrmionium, arXiv:1904.06870.

[50] R. Zarzuela and Y. Tserkovnyak, Antiferromagnetic textures and dynamics on the surface of a heavy metal, Phys. Rev. B **95**, 180402(R) (2017).

[51] L. Shen, J. Xia, G. Zhao, X. Zhang, M. Ezawa, O. A. Tretiakov, X. Liu, and Y. Zhou, Spin torque nano-oscillators based on antiferromagnetic skyrmions, Appl. Phys. Lett. **114**, 042402 (2019).

[52] L. Shen, J. Xia, X. Zhang, M. Ezawa, O. A. Tretiakov, X. Liu, G. Zhao, and Y. Zhou, Current-induced dynamics and chaos of an antiferromagnetic bimeron, arXiv:1905.09007.

[53] Y. A. Kharkov, O. P. Sushkov, and M. Mostovoy, Bound States of Skyrmions and Merons Near the Lifshitz Point, Phys. Rev. Lett. **119**, 207201 (2017).

[54] B. Göbel, A. Mook, J. Henk, I. Mertig, and O. A. Tretiakov, Magnetic bimerons as skyrmion analogues in in-plane magnets, Phys. Rev. B **99**, 060407(R) (2019).

[55] E. G. Tveten, T. Müller, J. Linder, and A. Brataas, Intrinsic magnetization of antiferromagnetic textures, Phys. Rev. B **93**, 104408 (2016).

[56] S. Rohart and A. Thiaville, Skyrmion confinement in ultrathin film nanostructures in the presence of Dzyaloshinskii-Moriya interaction, Phys. Rev. B **88**, 184422 (2013).

[57] I. Dzyaloshinsky, A thermodynamic theory of "weak" ferromagnetism of antiferromagnetics, J. Phys. Chem. Solids **4**, 241 (1958).

[58] T. Moriya, Anisotropic superexchange interaction and weak ferromagnetism, Phys. Rev. **120**, 91 (1960).

[59] H. V. Gomonay and V. M. Loktev, Spin transfer and current-induced switching in antiferromagnets, Phys. Rev. B **81**, 144427 (2010).

[60] See Supplemental Material at http://link.aps.org/supplemental/10.1103/PhysRevApplied.12.064033 for the detailed results of micromagnetic simulations on AFM skyrmions and skyrmioniums, which cites Refs. [33,55,56,61].

[61] A. Vansteenkiste, J. Leliaert, M. Dvornik, M. Helsen, F. Garcia-Sanchez, and B. Van Waeyenberge, The design and verification of MuMax3, AIP Adv. **4**, 107133 (2014).

[62] E. G. Tveten, A. Qaiumzadeh, O. A. Tretiakov, and A. Brataas, Staggered Dynamics in Antiferromagnets by Collective Coordinates, Phys. Rev. Lett. **110**, 127208 (2013).

[63] J. Mulkers, M. V. Milošević, and B. Van Waeyenberge, Cycloidal versus skyrmionic states in mesoscopic chiral magnets, Phys. Rev. B **93**, 214405 (2016).

[64] A. A. Thiele, Steady-State Motion of Magnetic Domains, Phys. Rev. Lett. **30**, 230 (1973).

[65] O. A. Tretiakov, D. Clarke, G. W. Chern, Y. B. Bazaliy, and O. Tchernyshyov, Dynamics of Domain Walls in Magnetic Nanostrips, Phys. Rev. Lett. **100**, 127204 (2008).

[66] D. J. Clarke, O. A. Tretiakov, G. W. Chern, Y. B. Bazaliy, and O. Tchernyshyov, Dynamics of a vortex domain wall in a magnetic nanostrip: Application of the collective-coordinate approach, Phys. Rev. B **78**, 134412 (2008).

[67] J. Iwasaki, W. Koshibae, and N. Nagaosa, Colossal spin transfer torque effect on skyrmion along the edge, Nano Lett. **14**, 4432 (2014).

[68] S. Z. Lin, Dynamics and inertia of a skyrmion in chiral magnets and interfaces: A linear response approach based on magnon excitations, Phys. Rev. B **96**, 014407 (2017).

[69] S. Z. Lin, A. Saxena, and C. D. Batista, Skyrmion fractionalization and merons in chiral magnets with easy-plane anisotropy, Phys. Rev. B **91**, 224407 (2015).

[70] O. A. Tretiakov and O. Tchernyshyov, Vortices in thin ferromagnetic films and the skyrmion number, Phys. Rev. B **75**, 012408 (2007).

[71] J. Müller, Magnetic skyrmions on a two-lane racetrack, New J. Phys. **19**, 025002 (2017).

[72] W. Kang, C. Zheng, Y. Huang, X. Zhang, Y. Zhou, W. Lv, and W. Zhao, Complementary skyrmion racetrack memory with voltage manipulation, IEEE Electron Devices Lett. **37**, 924 (2016).

[73] P. Lai, G. P. Zhao, F. J. Morvan, S. Q. Wu, and N. Ran, Motion of skyrmions in well-separated two-lane racetracks, Spin **7**, 1740006 (2017).

[74] S. Zhang, J. Wang, Q. Zheng, Q. Zhu, X. Liu, S. Chen, C. Jin, Q. Liu, C. Jia, and D. Xue, Current-induced magnetic skyrmions oscillator, New J. Phys. **17**, 023061 (2015).

[75] F. Garcia-Sanchez, J. Sampaio, N. Reyren, V. Cros, and J. V. Kim, A skyrmion-based spin-torque nano-oscillator, New J. Phys. **18**, 075011 (2016).

[76] Y. Zhou, E. Iacocca, A. A. Awad, R. K. Dumas, F. C. Zhang, H. B. Braun, and J. Akerman, Dynamically stabilized magnetic skyrmions, Nat. Commun. **6**, 8193 (2015).

[77] C. Jin, J. Wang, W. Wang, C. Song, J. Wang, H. Xia, and Q. Liu, Array of Synchronized Nano-Oscillators Based on Repulsion between Domain Wall and Skyrmion, Phys. Rev. Appl. **9**, 044007 (2018).